Journal of Colloid and Interface Science 437 (2015) 297–303

Contents lists available at ScienceDirect

Journal of Colloid and Interface Science

www.elsevier.com/locate/jcis

Surface loading effects on orthophosphate surface complexation at the goethite/water interface as examined by extended X-ray Absorption Fine Structure (EXAFS) spectroscopy

Dalton Belchior Abdala [a,*], Paul Andrew Northrup [b], Yuji Arai [c], Donald Lewis Sparks [d]

[a] Plant & Soil Sciences Department, University of Delaware, Newark, DE 19716, United States
[b] Stony Brook University, National Synchrotron Light Source, Brookhaven National Laboratory, Upton, NY 11973, United States
[c] Department of Natural Resources and Environmental Sciences, University of Illinois at Urbana-Champaign, Urbana, IL 61801, United States
[d] Department of Plant & Soil Sciences and Delaware Environmental Institute, University of Delaware, Newark, DE 19716, United States

ARTICLE INFO

Article history:
Received 17 July 2014
Accepted 19 September 2014
Available online 30 September 2014

Keywords:
Phosphorus solid-state speciation
Phosphorus surface complexation
Phosphorus K-edge EXAFS
Phosphorus retention mechanisms

ABSTRACT

To investigate the effect of P surface loading on the structure of surface complexes formed at the goethite/water interface, goethite was reacted with orthophosphate at P concentrations of 0.1, 0.2, and 0.8 mmol L^{-1} at pH 4.5 for 5 days. The P concentrations were chosen to ensure that P loadings at the surface would allow one to follow the transition between adsorption and surface precipitation. Extended X-ray Absorption Fine Structure (EXAFS) spectra were collected in fluorescence mode at the P K-edge at 2150 eV. The structural parameters were obtained through the fits of the sorption data to single and multiple scattering paths using Artemis. EXAFS analysis revealed a continuum among the different surface complexes, with bidentate mononuclear (^{2}E), bidentate binuclear (^{2}C) and monodentate mononuclear (^{1}V) surface complexes forming at the goethite/water interface under the studied conditions. The distances for P–O (1.51–1.53 Å) and P–Fe (3.2–3.3 Å for bidentate binuclear and around 3.6 Å for mononuclear surface complexes) shells observed in our study were consistent with distances obtained via other spectroscopic techniques. The shortest P–Fe distance of 2.83–2.87 Å was indicative of a bidentate mononuclear bonding configuration. The coexistence of different surface complexes or the predominance of one sorption mechanism over others was directly related to surface loading.

1. Introduction

The combination of strong binding of phosphorus (P) in soils, leading to its limited availability to plants, particularly, in highly weathered soils of the tropics, and the dependence of agriculture upon such soils for food production has motivated researchers to examine the sorption mechanisms of P in soils and soil components. From an environmental standpoint, issues surrounding excess P, often due to the disposal of P-rich agricultural byproducts to agricultural lands, have also prompted researchers to address the chemical reactions controlling the reactivity and transport of this element [1–5].

The adsorption phenomenon involving oxyanions and soil mineral oxides was originally thought to be characterized by an exchange reaction, which took place on the surface of soil minerals like Fe and Al (hydr)oxides. Early investigations aimed at understanding P bioavailability observed that phosphate exhibited some hysteresis and that behavior was attributed to the formation of more thermodynamically stable quasichemical entities or surface complexes. Elucidation of the surface complexes was speculative and inferred from multiple linear portions of the Langmuir plot, which were attributed to sites of varying reactivity [6,7]. Hingston et al. [8–11] studied the sorption of several oxyanions, including P, As and S, on goethite and gibbsite and concluded that the elemental selectivity of sorption was indeed due to specific sorption. It was only with the help of molecular-scale techniques that the lack of molecular descriptions of the surface complexes was fulfilled, bonding configurations corresponding to the different sorption mechanisms were first observed and chemisorption reactions were shown to be involved [12].

Over the past decades, solid-phase speciation studies of P have relied largely on the use of spectroscopic techniques, especially Fourier transform infra-red (FTIR) [13–18] and Nuclear Magnetic Resonance (NMR) [19–23] spectroscopies. A number of studies have been conducted to elucidate the sorption mechanisms and surface complexation/precipitation dependence on environmental

* Corresponding author at: Brazilian Synchrotron Light Laboratory, Rua Giuseppe Maximo Scolfaro, 10 000 – Campinas, 13 083-970 SP, Brazil.
E-mail address: daltonabdala@gmail.com (D.B. Abdala).

http://dx.doi.org/10.1016/j.jcis.2014.09.057
0021-9797/

conditions, particularly pH and P loading. Overall, and regardless of the technique employed, there seems to exist a consensus that the possible bonding configurations between phosphate and Fe and Al (hydr)oxides include bidentate binuclear (^{2}C) and monodentate mononuclear (^{1}V) structures (Table 1). Nevertheless, interpretations of surface complex structures, such as whether monodentate or bidentate complexes form, and the conditions at which they form are not clear. In terms of goethite, Infrared (IR) studies have suggested that an inner-sphere bidentate binuclear surface complex may be the predominant mechanism at low pHs [13,17] and low surface loading [23]. Kwon and Kubicki [24] employed MO/DFT calculations to model surface complexes and their findings corroborate the above studies. In a novel study employing NMR to address P sorption to Fe (hydr)oxides, Kim et al. [22] studied the bonding mechanisms of P over a wide range of P concentration (0.1–3 mM) and pH (3–11) that encompasses most of the previous studies. They observed that a bidentate binuclear complex was formed regardless of environmental conditions. However, a monodentate mononuclear surface complex has also been suggested at low pHs [14] and at high P loadings [23]. IR studies on other Fe (hydr)oxides include the work on ferrihydrite by Arai and Sparks [15], in which the authors have suggested that bidentate binuclear surface complexes that formed at pH 4–6 were protonated and unprotonated complexes formed at pH $\geqslant$ 7.5. Elzinga and Sparks [16], working with hematite, observed the formation of bidentate binuclear structures at lower pHs and higher surface loadings in the 3.5–7.0 pH range whereas, at the highest pH values studied (8.5–9.0), a monodentate mononuclear complex was present and its importance increased with increasing surface coverage at high pH values. It is worth pointing out that the controversies surrounding the accurate determination of sorption mechanisms are due to the lack of direct evidence together with the reliance of the molecular assignments on an analytical approach [25,26]. An additional aspect that most of the early studies fail to precisely address is the formation of surface precipitates [15] i.e., three dimensional entities formed when further increases in sorbate concentration exceeds a monolayer coverage on the mineral surface. A vast literature on this topic indicates that surface loading has a pronounced effect on the continuum between surface complexation and surface precipitation on a number of soil minerals and environmentally important elements [27–33]. At high P concentrations, surface precipitation may be catalyzed leading to a new solid phase that is less readily dissolved or desorbed. According to Sparks [34], surface complexation tends to dominate at low surface coverages. As surface coverage increases, nucleation is operational and results in the formation of distinct entities or aggregates on the surface. As surface loadings increase further, surface precipitation becomes the dominant mechanism.

Synchrotron-based X-ray absorption spectroscopy (XAS) has been extensively applied to model systems to resolve molecular-level sorption mechanisms of a number of soil contaminants [15,35,36]. These tools can greatly improve our understanding of P reactions in soils and provide predictions on an atomic/molecular basis of mechanisms of P retention on soil minerals. Such data are useful in the development of molecular sorption models if one aims to relate P speciation to P mobilization. Whereas the use of state-of-the-art techniques, such as XAS (XANES and EXAFS) can enhance our knowledge on the reaction processes that elements undergo in the environment, some limitations may constrain their widespread use. When it comes to EXAFS analysis of low-Z elements such as P, fluorescence yield decreases with decreasing atomic number, which is reflected in the poor signal:noise. This ultimately hinders the collection of high quality data. In addition, in dilute samples, e.g., environmental samples, fluorescence attenuation is severely augmented especially in a dense, high-Z matrix such as goethite.

It is noteworthy to mention that [37–39] employed XANES to distinguish P adsorption from surface precipitation at mineral/water interfaces. However, in their studies, the authors relied on indirect observations to address the bonding configurations of

Table 1
Relevant studies on the P sorption mechanisms formed at mineral (hydr)oxide surfaces using MO/DFT, ATR-FTIR, CIR-FTIR, NMR and XANES spectroscopies.

Surface complex	Technique	Surface loading, (μmol m^{-2})*, (mmol L^{-1})**, (mmol kg^{-1})*** or P/Fe****	Sorbent	References
Monodentate				
	CIR-FTIR	high, >>17****	Goethite	Tejedor-Tejedor and Anderson [13]
	ATR-FTIR	0.4**	Goethite	Persson et al. [14]
		high, ~0.5**	Hematite	Elzinga and Sparks [16]
	MO/DFT	high, >>1.5*	Goethite	Rahnemaie et al. [23]
	NMR	0.1–100**	Boehmite	Kim and Kirkpatrick [20]
Bidentate				
	CIR-FTIR	low, << ~0.2	Goethite	Tejedor-Tejedor and Anderson [13]
		initial conc. ~5**	TiO_2	Connor and McQuillan [55]
	ATR-FTIR	0.38–2.69*	Ferrihydrite	Arai and Sparks [15]
		initial conc. ~0.06**	Goethite	Luengo et al. [17]
		>~0.2*	Goethite	Antelo et al. [2]
		low ~0.005**	Hematite	Elzinga and Sparks [16]
	MO/DFT	low < 1.5*	Goethite	Rahnemaie et al. [23]
	ATR-FTIR, planewave/DFT	0.1**	Goethite	Kubicki et al. [56]
	NMR	0.1–150*	Boehmite and γ-alumina	Kim and Kirkpatrick [20]
		0.1–1.0**	Boehmite	Li et al. [21]
		0.1–3.0**	Akaganeite, boehmite, lepidocrocite	Kim et al. [22]
	NMR, ATR-FTIR, MO/DFT	2.6–26*	α-Al_2O_3	Li et al. [57]
	NMR	0.15–150*	Boehmite, corundum, gibbsite, bayerite and γ-alumina	Li et al. [58]
	XANES	750***	Ferrihydrite	Khare et al. [39]
		300–830***	Boehmite	

* Expresses phosphorus surface loadings in (μmol m^{-2}).
** Expresses phosphorus surface loadings in (mmol L^{-1}).
*** Expresses phosphorus surface loadings in (mmol kg^{-1}).
**** Expresses Fe/P ratios.

the surface structures being formed on the mineral surface, namely, the full width at half maximum height (FWHM) concept and extended Hückel calculations. Therefore, to the best of our knowledge, our study is the first to employ EXAFS to collect direct information on the P sorption mechanisms formed at the mineral/water interface.

Accordingly, we combined a batch technique with EXAFS spectroscopy to examine the effects of surface loading and pH on the local atomic environment of sorbed P at the goethite/water interface.

2. Material and methods

2.1. Mineral synthesis

Goethite was synthesized according to the method of Schwertmann and Cornell [40]. Briefly, 200 mL of 1 M $Fe(NO_3)_3$. $9H_2O$ was added to a plastic flask with continuous stirring and then 360 mL of 5 M KOH were carefully added. Four L of DDI water were added and the mixture was thoroughly mixed for 30 min. The flask was sealed with Scotch duct tape and placed in an oven set at 70 °C for 4 days. After the 4th day, the supernatant solution was poured off and the goethite precipitate, which had settled to the bottom of the container, was washed with dialysis tubing for about one week until the electric conductivity matched that of the distilled deionized water (~0.95 μS cm^{-1}). The dialyzed mineral was transferred into 50 mL centrifuge tubes and centrifuged at 11,000 rpm for 30 min. The supernatant was removed with a syringe and the precipitate was freeze dried for approximately 60 h. Finally, the material was softly ground in a mortar and stored in a polystyrene bottle.

The specific surface area of the goethite, determined by a three point Brunauer–Emmett–Teller N_2 gas adsorption isotherm, was 40.0 ± 0.6 m^2 g^{-1}.

2.2. Sorption experiments

Centrifuge tubes containing stock goethite suspensions of 20 g L^{-1} were placed in a rotating shaker set at 30 rpm at 298 K and equilibrated in 50 mmol L^{-1} KCl with the pH adjusted to 4.5 for 36 h prior to phosphate addition. The pH in the suspensions was monitored throughout the shaking period and adjusted to the target pH as needed by the addition of either NaOH or HCl. Thereafter, an aliquot of the suspension was transferred to a new centrifuge tube to yield a goethite suspension of 2 g L^{-1}, and a phosphate solution of 0.1, 0.2, and 0.8 mmol L^{-1} was added. This corresponded to surface coverages of 1.25, 2.5 and 10 μmol m^{-2}. The tubes were shaken and 5 mL aliquots from each tube were sampled on the 5th day.

The phosphate concentrations were carefully chosen to ensure a range of surface coverages. The reaction time, 5 days, was shown to be sufficient to ensure that the bulk of the added P (>95%) was associated with the surface.

2.3. XAS sample preparation and analysis

Each sample was immediately filtered to pass through a 0.22 μm nitrocellulose membrane filter and washed three times with 3 mL of pH adjusted 50 mmol L^{-1} KCl to remove any entrained phosphate not associated with the surface. The cellulose membrane filter containing the mineral paste was sealed with 5-micron polypropylene XRF thin film (Ultralene®) and stored moist in a sealed sample box at 6 °C until analysis. The samples were stored for no more than 24 h prior to analysis. Phosphorus K-edge spectra (2150 eV) were collected at beamline X15B at the National Synchrotron Light Source (NSLS) at Brookhaven National Laboratory. The X15B sample chamber is a "hutch box" containing a He atmosphere at 1.001 atm positive pressure.

EXAFS spectra were collected in fluorescence mode with samples mounted at 45° to the incident beam, using a liquid-nitrogen-cooled Canberra Ultra-Low-Energy Germanium detector positioned at 90°. X15B beamline optics consist of a collimating and harmonic-rejection mirror, a monochromator utilizing Si (1 1 1) crystals to tune energy, and a focusing mirror to gather approximately 5×10^{11} photons s^{-1} into a 1-mm spot at the sample position. The fluorescence signal was normalized to incident beam intensity as measured using a windowless ionization chamber. XAS spectra were collected at photon energies between 2099 and 2750 eV with a minimum step size of 0.1 eV across the edge and gradually increasing step sizes up to 6 eV at 2750 eV. The collected spectra were processed using the Athena software in the computer package IFEFFIT [41]. Six to ten individual spectra were averaged for each sample.

2.3.1. EXAFS data analysis

The averaged spectra were normalized to an atomic absorption of one, and the EXAFS signal was extracted from the raw data using linear pre-edge and a quadratic spline post-edge, followed by subtraction of background using the Autobk algorithm [42]. Data were converted from energy to photo electron momentum (k-space) and k-weighted by k^2. Fourier transforms (FT) of the k^2-weighted EXAFS were calculated over a k-range of 2.0 to between 10.1 and 10.6 to obtain the R-space. The FT of the EXAFS was fit with the predicted neighbor paths by varying the number of coordinating atoms (CN), their distance (ΔR), mean square displacement (δ^2) and passive electron reduction factor (S_0^2) in order to obtain the best fit between the experimental and predicted spectra.

First shell (P–O) bond distances were obtained from the literature from crystallographic data and were used in the fit and fixed at these values for higher shell fitting. We fixed the CN of the first oxygen shell at 4 as the regular coordination environment of PO_4 ions. Fits to second neighbor Fe shells were made by setting the degeneracy of each surface complex, CN = 2 for bidentate binuclear or CN = 1 for either bidentate mononuclear or mononuclear coordination, and fitting an amplitude factor describing the fraction of P in each configuration. One may argue about the method used to fit first and second coordination shells, that is, by setting the CN instead of floating it, as is standard practice. Indeed, floating CN was our first approach. However, the misfit between data and fit was large enough to consider the approach we used. As a matter of fact, constraining some parameters during fitting of EXAFS data is not unusual in the literature [54,59,60]. Yet, in order to address our fitting strategy, we tested our fits by varying coordination numbers upon finding a reasonable goodness of fit for a given fit performed to second coordination shells. Lastly, to make best use of the data we collected, we found it appropriate to set CNs for each coordination shell, fit the data and to rely on existing information from related techniques.

Spectra of an aqueous solution of 10 mmol L^{-1} KH_2PO_4 at pH 4.5 ($P_{(aq)}$) were collected and fit to confirm the position of the multiple scattering (MS) within the PO_4 tetrahedron. The inclusion of MS improved the fit in the 1.6–2.8 Å region as strong MS within the PO_4 tetrahedron was expected. We included three MS paths in our fits: namely three-legged P–O1–O2–P triangular (MS_1), four-legged P–O1–PO2–P non collinear (MS_2) and four-legged P–O1–P–O1–P collinear (MS_3) paths.

Several different models were employed to fit the MS path, including (i) correlating σ^2 MS to 2 times that of the single scattering (SS) path; and (ii) a direct correlation between σ^2 MS and that of the SS path [43].

3. Results and discussion

There have been a number of previous studies using spectroscopic techniques to characterize phosphate surface complexes forming on Fe(III)-, Al- and Ti (hydr)oxide mineral surfaces, including MO/DFT and ATR-FTIR, CIR-FTIR, NMR and XANES spectroscopies. Unlike IR spectroscopy, EXAFS analysis is insensitive to the protonation environment of surface complexes. Therefore, our discussion will be limited to the bonding configuration of the surface species. In terms of bonding configuration, the bidentate binuclear configuration seems to be the most favorable P sorption complex formed at the (hydr)oxides surface (Table 1; [12,44,45]). Yet, what has not been established in the literature related to P bonding configurations at mineral surfaces are the environmental conditions which favor formation of a particular sorption complex mechanism. Additionally, the majority of the studies have employed NMR and IR techniques. There are no reports in the literature using EXAFS where detailed structural information, such as next nearest neighbor, bond distance and coordination numbers are reported. A list of relevant studies on P sorption mechanisms formed at mineral (hydr)oxides surfaces is shown in Table 1 and is aimed at assisting in the discussion of our results.

3.1. P-EXAFS spectra

In this study, XANES data are not presented as differences in $\mu(E)$ among spectra are very subtle. Fig. 1 shows the experimental Fourier Transform results of EXAFS data of goethite spiked with P at surface coverages of 1.25, 2.5 and 10 μmol m^{-2} at pH 4.5. The *R*-space is a result of the Fourier transformation of the $\chi(k)$ function. The peaks shown in the experimental $\chi(k)$ spectra are related to the coordination shells formed between P–O and P–Fe and reflect the interatomic distances within the material. For all samples, the E_0 ranged from −2.28 to 0.96 eV. The contributions of O were localized at P–O distances ranging from 1.51 to 1.53 Å and MS dominates at ~2.75 to 2.78 Å. The P–Fe shells are indicative of the existence of three different bonding configurations between P and the goethite surface and will be treated separately in the following discussion.

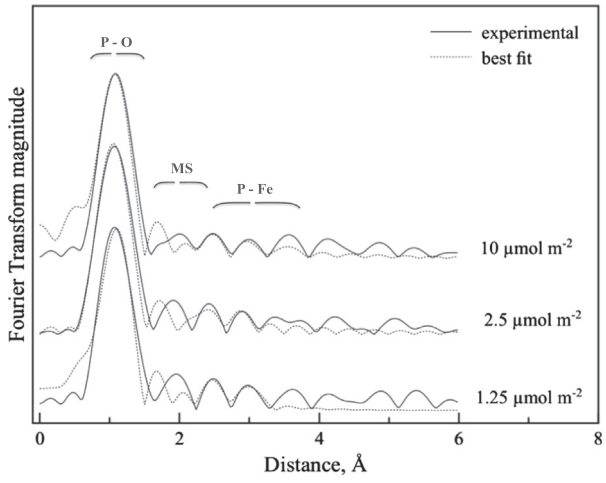

Fig. 1. Experimental (solid line) and best fit (dashed line) Fourier transformed spectra of the phosphate surface complexes formed at the goethite/water interface at pH 4.5. A change in spectrum shape (R-space) followed by an increase in the phosphate loading indicates that the phosphate surface speciation changes with surface loading. Braces are intended to show the approximate region where the P–O, multiple scattering (MS) and P–Fe shells most significantly contribute in radial distance in the Fourier transformed spectra.

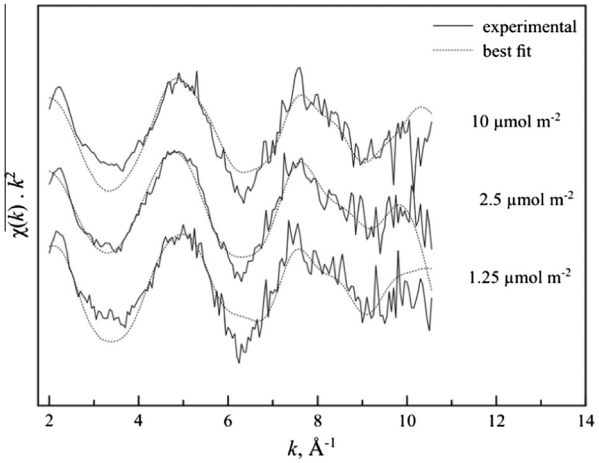

Fig. 2. Experimental (solid line) and best-fit (dashed line) k^2-weighted back-transformed spectra of phosphate sorbed on goethite at 1.25, 2.5 and 10 μmol m^{-2} at pH 4.5.

Fig. 2 shows the k^2-weighted EXAFS spectra of P sorbed on goethite. The structural parameters obtained from the linear least-square fits are presented in Table 2. A fit was accepted whenever the *R*-factor value for a given Fourier transform part, reported either in Fourier transform magnitude, real (*R*) or back-transformed *k*-space data (*q*), was less than 6%. That is, the misfit between data and best fit. Figs. 4 and 5 show the Real (*R*) and (*q*) parts of the Fourier transform of P sorbed on goethite, respectively, at three different surface coverages, 1.25, 2.5 and 10 μmol m^{-2}.

3.2. Overall formation of P surface complexes at the goethite/water interface

We have identified the formation of three different phosphate surface complexes at the goethite/water interface, namely bidentate mononuclear (^{2}E), bidentate binuclear (^{2}C) and monodentate mononuclear (^{1}V) surface complexes. Additionally, surface precipitates were also observed, particularly, at higher P loadings.

The shortest P–Fe distances of 2.87–2.83 Å are indicative of a bidentate mononuclear configuration between P and Fe at low and intermediate surface loadings, respectively. Intermediate P–Fe distances of 3.27, 3.3 and 3.3 Å were characteristic of a bidentate binuclear configuration between P and Fe at low, intermediate and high surface loadings, respectively. The most distant shell, 3.6 Å, was indicative of a linear configuration between P and Fe. Table 2 shows the P–O and P–Fe bonding distances and corresponding P sorption mechanisms.

3.3. Adsorption complexes

As indicated in Table 2, our results show that bidentate (^{2}C and ^{2}E) surface complexes are predominantly formed at low surface coverages and transition to monodentate configuration as surface coverage increases. This seems consistent with the literature that indicated that low surface coverages favor the formation of bidentate surface complexes [12,13,16,20,23,44–47] and that the relative importance of bidentate binuclear species decreases as surface loading increases such that monodentate configuration would predominate at higher surface loadings [13,23]. However, on the basis of ATR-FTIR analysis, [18,48] observed that P adsorbs mainly as bidentate complexes at high phosphate loadings and that monodentate surface complexes begin to be important at low phosphate loadings and at high pHs. This was ascribed to bidentate species locating more charge at the surface than mono-

Table 2
P–O and P–Fe bonding distances, surface complex distribution and corresponding bonding configurations of P on goethite at three different surface coverages.

Surface loading	P–O		Surface complexes								
			Bidentate mononuclear			Bidentate binuclear			Monodentate		
μmol m^{-2}	*R* (Å)	σ^2	*R* (Å)	σ^2	Fraction (%)	*R* (Å)	σ^2	Fraction (%)	*R* (Å)	σ^2	Fraction (%)
1.25	1.51 (±0.01)	0.0021	2.87 (±0.03)	0.0032	48	3.27 (±0.06)	0.0033	47			
2.5	1.52 (±0.01)	0.0004	2.83 (±0.04)	0.0052	77	3.3 (±0.08)	0.0030	25			
10	1.51 (±0.01)	0.0004				3.3 (±0.05)	0.0002	18	3.6 (±0.04)	0.0035	63

R: radial structure function (RSF); σ^2: mean square displacement, (): uncertainties associated with parameter estimates. The bold values refer to the surface loadings, expressed in μmol m^{-2}, employed in our study.

dentate species, producing a lower electrostatic repulsion between the adsorbed species in the 1-plane. Interestingly, the observation of [18,48] is consistent with the behavior of arsenic in its pentavalent form (As(V)), an analog of phosphate, having similar chemical and geometric properties, and present as the ionic species, $H_2AsO_4^-$ and $H_2PO_4^-$, respectively, at the typical pH range in the environment.

Because there has not been any EXAFS study on orthophosphate bonding on mineral (hydr)oxides, we compared our results to studies relying on (i) MO/DFT and planewave/DFT calculations performed by [23,24,56] on phosphate sorbed to Fe-oxides and on (ii) EXAFS of As(V) sorbed on mineral (hydr)oxides. Table 3 shows the P–O and P–Fe bonding distances, surface complex distribution and corresponding bonding configurations of P on goethite as examined by EXAFS and obtained by MO/DFT and planewave/DFT calculations. On an average basis, our EXAFS observations were in good agreement with the calculated values, particularly for P–O, where interatomic distances varied within 0.05–0.1 Å. Likewise, the differences in P–Fe bond lengths for a bidentate binuclear configuration were small, varying between 0.04 and 0.07 Å. P–Fe distances for a monodentate configuration showed the largest divergence among the two approaches, approximately 0.2 Å. With EXAFS studies on As(V), it was observed that As(V) can form three bonding configurations with mineral (hydr)oxides surfaces, similarly to what was observed in our study [49,50]. However, counter to what was observed by these authors, our results show a predominance of the bidentate corner-sharing (^{2}C) surface complex at lower surface coverages and a transition to edge-sharing (^{2}E) and monodentate corner-sharing (^{1}V) as surface coverage increased to 10 μmol m^{-2}. A conceptual model depicting the surface loading effect on P surface complexation according to P-EXAFS analysis of sorption data from our study is shown in Fig. 3.

Table 3
P–O and P–Fe bonding distances, surface complex distribution and corresponding bonding configurations of P on goethite as examined by EXAFS and obtained by MO/DFT calculations from Kwon and Kubicki [24], Rahnemaie et al. [23] and planewave/DFT calculations by Kubicki et al. [56]. The values shown on the table correspond to the average of each individual value for a given surface complex.

Surface complex	EXAFS[1]		Kwon and Kubicki, [24]		Rahnemaie et al., [23]		Kubicki et al., [56]	
	P–O	P–Fe	P–O	P–Fe	P–O	P–Fe	P–O	P–Fe
Å								
Monodentate	1.51	3.6	1.57	3.37	1.61	3.6	1.56	3.42 (3.25–3.55) [3]
Bidentate binuclear	1.51	3.28	1.59	3.21	1.6	3.24	1.56	3.28 (3.18–3.45) [3]
Bidentate mononuclear	1.52	2.85	NO[2]	NO[2]	NO[2]	NO[2]	NO[2]	NO[2]

[1] Bond distances represent an average for the three surface loadings in Table 2.
[2] NO: Not observed.
[3] The numbers in parenthesis indicate the range of P–Fe bond lengths found by Kubicki et al., [56].

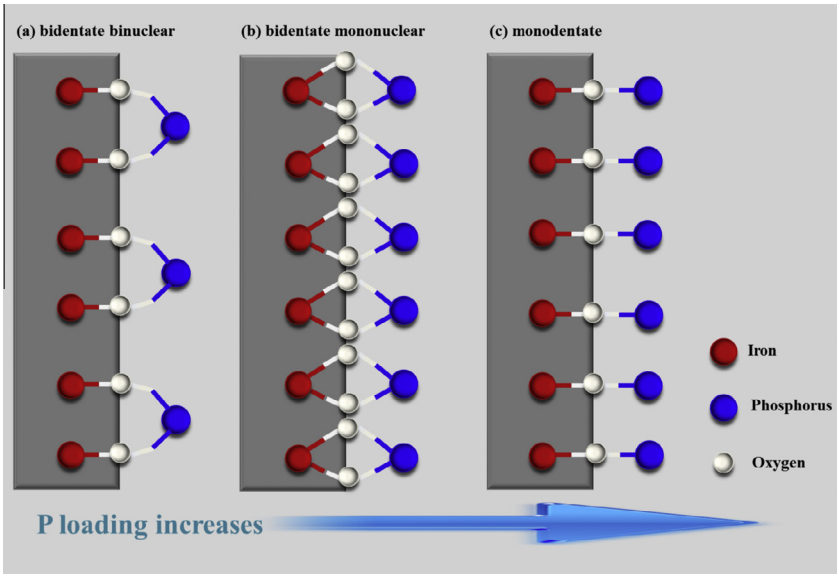

Fig. 3. Conceptual model depicting the surface loading effect of P on surface complexation at the goethite/water interface as determined by P-EXAFS analysis of sorption data.

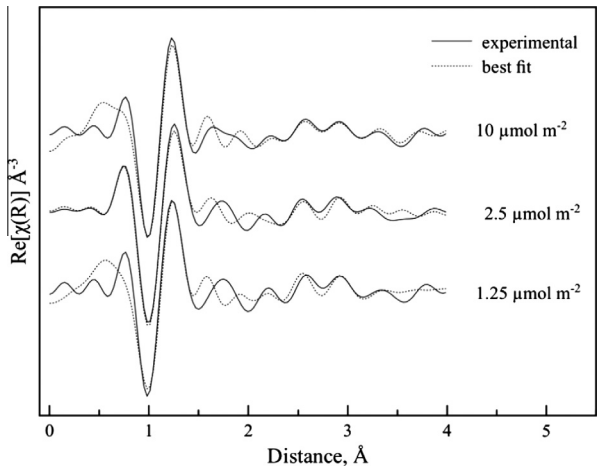

Fig. 4. Real (R) part of the Fourier Transform of P sorbed on goethite at three different surface coverages, 1.25, 2.5 and 10 μmol m^{-2}.

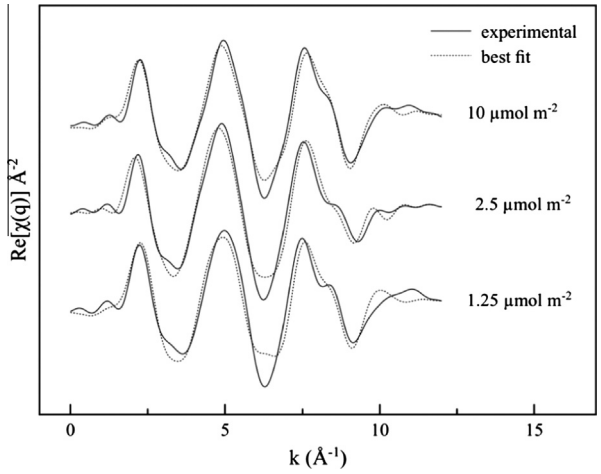

Fig. 5. Real (q) part of the Fourier Transform of P sorbed on goethite at three different surface coverages, 1.25, 2.5 and 10 μmol m^{-2}.

3.3.1. Bidentate mononuclear configuration

The shortest P–Fe distances, 2.83 and 2.87 Å, represent an edge sharing between the phosphate tetrahedra and the Fe octahedra. Thus, the only possible configuration for such a short distance would be an edge-sharing bidentate mononuclear configuration (^{2}E). EXAFS spectroscopy has indicated that a bidentate mononuclear configuration (^{2}E) can be formed between tri-, tetra- and penta-valent metals and (hydr)oxide surfaces, such as As(V) on goethite [48,49], Se(IV) on HMO [50], As(III) on ferrihydrite and on hematite [51] and As(III) on maghemite [52] under different experimental conditions.

However, since the existence of a bidentate mononuclear surface complex between P and (hydr)oxide minerals has never been observed, we tried to rule out its existence by calculating it as forming a 120° angle. In this case, the P–Fe bond distance would be 3.15 Å. We also considered that MS contributions could be substantially affecting *R* at those distances, but this hypothesis was promptly discarded after MS from an aqueous orthophosphate sample (10 mmol L^{-1} as KH_2PO_4 at pH 4.5) showed MS contributions at around ~2.74 Å.

Furthermore, the P–Fe distances observed in our study are comparable to those observed in the above-mentioned EXAFS studies, 2.83–2.87 Å and 2.87–3.08 Å, respectively (reported distances include uncertainties associated with the measure).

3.3.2. Bidentate binuclear configuration

A bidentate binuclear configuration (^{2}C) of phosphate on (hydr)oxides has been shown to be the predominant sorption mechanism formed at lower surface coverages. In this study, the ^{2}C surface complex was present, although at different proportions, across the entire surface coverage range. The rationale for why ^{2}C predominates at lower surface coverages is that this configuration should be favored when the Fe/P ratio is smaller than unity. It follows that at low P concentration, the sorption sites compete with the PO_4 molecules at the same strength such that one PO_4 molecule must equally satisfy as many sorption sites as possible. Therefore, ^{2}C forms first and because it is strongly bound to high affinity sorption sites, it has a large thermodynamic stability, thus remaining associated with the surface even as solution P concentration increases. In addition, at low pHs, i.e., pH ~ 4.5, a higher positive surface charge induces a higher adsorption capacity for anions like phosphate, because more negative charge can be brought to the surface for a given change in electrostatic potential [52].

Table 2 shows the surface complex distribution as a function of surface loading. Following the surface complex distribution across the loading range, one can observe that the overall percent distribution of ^{2}C remains constant (~50%) when the surface coverage increases by a factor of 2.

3.3.3. Monodentate configuration

Relatively few spectroscopic studies have reported P being attached to (hydr)oxide surfaces in a monodentate (^{1}V) configuration (Table 1). The studies in which a ^{1}V configuration has been observed were, in general, carried out employing P concentrations at relatively high surface coverages [13,16]. Whereas the P–Fe distances for bidentate binuclear configuration are in good agreement with the work by [23], who found P–Fe distances varying between 3.22 and 3.26 Å, the P–Fe distance for a monodentate configuration observed in our study was much larger, ~3.6 Å. Though, this is in agreement with the calculations performed by [24], who found P–Fe bond distances generally longer for either configuration, if $a \geqslant 170°$ angle is formed by P–O–Fe, suggesting a P–Fe bond distance of around 3.6 Å. EXAFS studies indicate that for As(V) these distances are generally in the order of 3.57–3.63 Å [48,53]. Since P is a much lighter element than As, it is possible that the repulsion of P by the Fe atoms tend to maintain P as far apart from Fe as possible, thus P–O–Fe forms preferentially a linear structure when a monodentate configuration is formed. Alternatively, the Fe–O bond distance may also be influenced by the repulsion and, accordingly, present a longer total Fe–P distance.

3.4. Environmental significance of our findings

In the highly weathered agricultural soils of the tropics, P is arguably the major limiting factor for crop production due to the high sorption capacity of these soils together with P's strong binding to mainly Al- and Fe-(hydr)oxide soil minerals. On the other hand, over-application of P fertilizers, particularly via application of organic amendments, has led to the buildup of soil P to levels at which P loss potential can be significantly increased [4,5]. Addressing how P surface complexation (SC) is affected by environmental conditions such as surface loading in acidic tropical soils represents a true challenge in terms of analytical methods. This is especially true in view of the limitations imposed by the techniques that have traditionally been employed, e.g., FTIR, for which utilization is constrained under pHs lower than 4.5 [21] (which is a soil pH range commonly found under tropical conditions) and ^{31}P NMR analysis in Fe-rich soils due to Fe paramagnetism [20].

Our P-EXAFS results represent an advance over the analytical limitations imposed by the above-mentioned techniques and provide direct evidence on the molecular basis for the low P

availability in acidic soils low in P as well as for the greater cycling potential of P in soils high in this element. In addition, the research shows the suitability of the EXAFS technique to study P surface complexation at mineral/water interfaces under conditions typically found in tropical soils, that is, at relatively low P concentrations (2.5 μmol L^{-1}, i.e., 77.5 mg kg^{-1}) and at low pHs, as EXAFS is insensitivity to the later.

Our results indicated that P was rapidly (<5 days) sorbed at the goethite surface, even at surface loadings above the P loadings predicted for monolayer coverage on goethite. Regardless of the P surface loadings employed in this study, P sorbed on goethite via a ligand exchange mechanism, that is, forming a quite stable surface complex. It was also observed that surface loading has a marked effect on surface complexation, which transitioned from bidentate binuclear into bidentate mononuclear or monodentate with increases in surface loading (Fig. 3). This continuum of binding mechanisms corroborates the vast literature indicating the thermodynamic feasibility for the formation of more stable structures at low surface coverages, where P availability is constrained due to the much higher binding energy involved [12,44–46]. In most acidic soils, the available P pool associated with soil minerals is usually low and only a small fraction of sorbed P is readily desorbable, most likely from solid phases formed from recent additions of fertilizer P or physically sorbed phosphate by less energetic binding. Over fertilization of P may, therefore, enhance P availability and mobility due to formation of monodentate surface complexes, which have a less energetic character, and are favored at high surface coverages.

Acknowledgments

The senior author gratefully acknowledges the receipt of a Delaware Environmental Institute (DENIN) graduate fellowship. The authors appreciate financial support from the U.S. National Science Foundation via Delaware EPSCoR. Support for this project was made possible by the Unidel Foundation and by Delaware EPSCoR with funds from the National Science Foundation Grant EPS-0814251. We also extend our thanks to the United States Department of Energy for providing us access to the National Synchrotron Light Source and for the technical support provided by the later.

References

[1] R.F. Novais, T.J. Smyth, Fósforo em solo e planta em condições tropicais, Universidade Federal de Viçosa, Viçosa, MG, 1999. 399p.
[2] J. Antelo, M. Avena, S. Fiol, R. Lopez, F. Arce, J. Colloid Interface Sci. 285 (2005) 476–486.
[3] J. Kruse, P. Leinweber, J. Plant Nutr. Soil Sci. 171 (2008) 613–620.
[4] D.B. Abdala, A.K. Ghosh, I.R. Silva, R.F. Novais, V. Alvarez, Agric. Ecosyst. Environ. 162 (2012) 15–33.
[5] D.B. Abdala, I.R. Silva, L. Vergütz, D.L. Sparks, Chemosphere 119 (2015) 504–514.
[6] C.R. Fried, G. Shapiro, Soil Sci. Soc. Am. Proc. 20 (1956) 471–475.
[7] S.R. Olsen, F.S. Watanabe, Soil Sci. Soc. Am. Proc. 21 (1957) 144–149.
[8] F.J. Hingston, R.J. Atkinson, A.M. Posner, J.P. Quirk, Congr. Soil Sci. Soc. 9th (Adelaide) (1968) 669–678.
[9] F.J. Hingston, A.M. Posner, J.P. Quirk, Disc. Faraday Soc. 52 (1971) 334–342.
[10] F.J. Hingston, J. Soil Sci. 23 (1972) 177–192.
[11] F.J. Hingston, J. Soil Sci. 25 (1974) 16–26.
[12] R.L. Parfitt, R.J. Atkinson, R. St, C. Smart, Soil Sci. Soc. Am. J. 39 (1975) 837–841.
[13] M.I. Tejedor-Tejedor, M.A. Anderson, Langmuir 6 (1990) 602–611.
[14] P. Persson, N. Nilsson, S. Sjoberg, J. Colloid Interface Sci. 177 (1996) 263–275.
[15] Y. Arai, D.L. Sparks, J. Colloid Interface Sci. 241 (2001) 317–326.
[16] E.J. Elzinga, D.L. Sparks, J. Colloid Interface Sci. 308 (2007) 53–70.
[17] C. Luengo, M. Brigante, J. Antelo, M. Avena, J. Colloid Interface Sci. 300 (2006) 511–518.
[18] J. Antelo, S. Fiol, C. Pérez, S. Mariño, F. Arce, D. Gondar, R. López, J. Colloid Interface Sci. 347 (2010) 112–119.
[19] W.F. Bleam, P.E. Pfeffer, S. Goldberg, R.W. Taylor, R.A. Dudley, Langmuir 7 (1991) 1702–1712.
[20] Y. Kim, R.J. Kirkpatrick, Eur. J. Soil Sci. 55 (2004) 243–251.
[21] W. Li, J. Feng, K.D. Kwon, J.D. Kubicki, B.L. Phillips, Langmuir 26 (2010) 4753–4761.
[22] J. Kim, W. Li, B.L. Philips, C.P. Grey, Energy Environ. Sci. 4 (2011) 4298–4305.
[23] R. Rahnemaie, T. Hiemstra, W.H. van Riemsdijk, Langmuir 23 (2007) 3680–3689.
[24] K.D. Kwon, J.D. Kubicki, Langmuir 20 (2004) 9249–9254.
[25] Y. Arai, D.L. Sparks, Adv. Agron. 94 (2007) 135–179.
[26] I. Carabante, M. Grahn, A. Holmgren, J. Hedlund, J. Colloid Interface Sci. 351 (2010) 523–531.
[27] L. Charlet, A. Manceau, J. Colloid Interface Sci. 148 (1992) 443–458.
[28] S. Fendorf, Geoderma 67 (1995) 55–71.
[29] A.M. Scheidegger, G.M. Lamble, D.L. Sparks, J. Colloid Interface Sci. 186 (1997) 118–128.
[30] A.M. Scheidegger, D.G. Strawn, G.M. Lamble, D.L. Sparks, Geochim. Cosmochim. Acta 62 (1998) 2233–2245.
[31] R.G. Ford, D.L. Sparks, Environ. Sci. Technol. 34 (2000) 2479–2483.
[32] D.R. Roberts, R.G. Ford, D.L. Sparks, J. Colloid Interface Sci. 263 (2003) 364–376.
[33] M. Nachtegaal, D.L. Sparks, J. Colloid Interface Sci. 276 (2004) 13–23.
[34] D.L. Sparks, Environmental Soil Chemistry, Second ed., Academic Press, 2002. 368p.
[35] B.A. Manning, S.E. Fendorf, S. Goldberg, Environ. Sci. Technol. 32 (1998) 2383–2388.
[36] J.D. Peak, D.L. Sparks, Environ. Sci. Technol. 36 (2002) 1460–1466.
[37] D. Hesterberg, W. Zhou, K.J. Hutchison, S. Beauchemin, D.E. Sayers, J. Synchrotron Rad. 6 (1999) 636–638.
[38] N. Khare, D. Hesterberg, J.D. Martin, Environ. Sci. Technol. 39 (2005) 2152–2160.
[39] N. Khare, J.D. Martin, D. Hesterberg, Geochim. Cosmochim. Acta 71 (2007) 4405–4415.
[40] U. Schwertmann, R.M. Cornell, Iron Oxides in the Laboratory: Preparation and Characterization, Wiley-VCH, Weinheim, Germany, 2000.
[41] B. Ravel, M. Newville, J. Synchrotron Rad. 12 (2005) 537–541.
[42] M. Newville, P. Livins, Y. Yacoby, J.J. Rehr, E.A. Stern, Phys. Rev. B Condens. Matter 47 (1993) 14126–14131.
[43] A.A. Rouff, M. Natchegaal, S. Rabe, F. Vogel, J. Phys. Chem. A 113 (2009) 6895–6903.
[44] R.L. Parfitt, Adv. Agron. 30 (1978) 1–50.
[45] R.L. Parfitt, Soil Sci. Soc. Am. Proc. 39 (1975) 837–841.
[46] R.L. Parfitt, R.J. Atkinson, Nature 264 (1976) 740–742.
[47] R.L. Parfitt, J.D. Russell, J. Soil Sci. 28 (1977) 297–305.
[48] P.R. Grossl, M.J. Eick, D.L. Sparks, S. Goldberg, C.C. Ainsworth, Environ. Sci. Technol. 31 (1997) 321–326.
[49] A. Foster, G.E. Brown, G.A. Parks, Geochim. Cosmochim. Acta 67 (2003) 1937–1953.
[50] G. Ona-Nguema, G. Morin, F. Juillot, G. Calas, G.E. Brown, Environ. Sci. Technol. 39 (2005) 9147–9155.
[51] G. Morin, G. Ona-Nguema, Y. Wang, N. Menguy, F. Juillot, O. Proux, F. Guyot, G. Calas, G.E. Brown Jr., Environ. Sci. Technol. 42 (2008) 2361–2366.
[52] T. Hiemstra. Surface complexation at mineral interfaces: Multisite and Charge Distribution approach. (Ph.D. thesis), Wageningen University, 2010.
[53] G.A. Waychunas, B.A. Rea, C.C. Fuller, J.A. Davis, Geochim. Cosmochim. Acta 57 (1993) 2251–2269.
[54] Y. Arai, E.J. Elzinga, D.L. Sparks, J. Colloid Interface Sci. 235 (2001) 80–88.
[55] P.A. Connor, A.J. McQuillan, Langmuir 15 (1999) 2916–2921.
[56] J.D. Kubicki, K.W. Paul, L. Kabalan, Q. Zhu, M.K. Mrozik, M. Aryanpour, A. Pierre-Louis, D.R. Strongin, Langmuir 28 (2012) 14573–14587.
[57] W. Li, Geochim. Cosmochim. Acta 107 (2013) 252–266.
[58] W. Li, X. Feng, Y. Yan, D.L. Sparks, B.L. Phillips, Environ. Sci. Technol. 15 (2013) 8308–8315.
[59] B.C. Bostick, S.E. Fendorf, Geochim. Cosmochim. Acta 67 (2003) 909–921.
[60] D. Sherman, S.R. Randall, Geochim. Cosmochim. Acta 67 (2003) 4223–4230.